Control Engineering Practice 57 (2016) 99–110

Contents lists available at ScienceDirect

Control Engineering Practice

journal homepage: www.elsevier.com/locate/conengprac

Multimode combustion in a mild hybrid electric vehicle. Part 1: Supervisory control

Sandro Nüesch *, Anna G. Stefanopoulou

Department of Mechanical Engineering in the University of Michigan, 2350 Hayward, Ann Arbor, MI48109, USA

ARTICLE INFO

Article history:
Received 14 December 2015
Received in revised form
1 June 2016
Accepted 3 September 2016
Available online 21 September 2016

Keywords:
Homogeneous charge compression ignition (HCCI) combustion
Mild HEV
Internal combustion engines
Powertrain control
Combustion mode switch
Supervisory control

ABSTRACT

This is the first of a two-part simulation study that discusses the application of a multimode combustion engine in a mild hybrid electric vehicle (HEV). The torque assist, offered by the electric motor, can be used to extend the residence time in the homogeneous charge compression ignition (HCCI) regime, before returning to spark-ignition (SI) combustion. To enable multimode operation in the HEV, the supervisory control strategy has to maintain the battery's state-of-charge while accounting for the SI/HCCI combustion mode switch. In this study four supervisors are discussed which extend the baseline equivalent consumption minimization strategy by the mode switching decision.

1. Introduction

Since the 1980s homogeneous charge compression ignition (HCCI) combustion has been an active area of research (Najt & Foster, 1983; Thring, 1989). The HCCI principle relies on a homogeneous and highly dilute charge auto-igniting, triggered by compression. This promises high benefits in efficiency due to its ability to operate unthrottled, increased thermal efficiency (Cairns & Blaxill, 2005), and reductions in timing losses (Farrell & Stevens, 2006). Furthermore, its low peak cylinder temperatures result in very low levels of engine-out NO_x. In contrast, however, elevated levels of HC and CO were seen (Dec & Sjöberg, 2003). HCCI operation can be enabled by several methods. In this article recompression HCCI (Willand, Nieberding, Vent, & Enderle, 1998) is applied. Variable valve timing (VVT) allows early closing of the exhaust valves to trap large amounts of highly reactive residual gas, which in turn promotes autoignition of the charge during the succeeding engine cycle. Due to the relatively inexpensive hardware this represents a cost-effective method to implement and control this combustion mode. Transient HCCI control has been discussed by Jade, Hellström, Larimore, Jiang, and Stefanopoulou (2016). They presented experiments for such a configuration, showing very fast and stable engine load and speed transitions while in HCCI mode.

A disadvantage of recompression HCCI, however, is its very narrow operating regime. At midload conditions, the very fast pressure rise rates result in ringing and potential hardware damage (Thring, 1989). On the other hand, at low loads not enough fuel energy is available to maintain stable combustion, resulting in increased occurrences of misfires (Hellström & Stefanopoulou, 2013). During common drive cycles the driver regularly demands engine loads and speeds outside the feasible HCCI regime. This can be resolved by combining HCCI with spark ignition (SI) combustion in a multimode engine as described by Kulzer et al. (2007). To analyze the potential of such an engine in terms of fuel economy, Cairns and Blaxill (2005), Kulzer et al. (2007), Ma, Zhao, Li, and Ladommatos (2001), and Ortiz-Soto, Assanic, and Babajimopoulos (2012) applied steady-state engine maps for SI and HCCI in drive cycle simulations. In addition, to prolong the residence time in HCCI mode while reducing the number of mode switches, this SI/HCCI multimode concept was extended to different types of hybrid electric vehicles (HEV) by Delorme et al. (2010), Lawler, Ortiz-Soto, Gupta, Peng, and Filipi (2011), and Ahn, Whitefoot,

Abbreviations: ECMS, Equivalent consumption minimization strategy; ECU, Engine control unit; HCCI, Homogeneous charge compression ignition; HEV, Hybrid electric vehicle; ISG, Integrated starter-generator; SI, Spark-ignited; SOC, State-of-charge; *Bsl*, Baseline; *Ext*, Extended; *Max*, Maximum; *Opt*, Optimal; *Ph*, Phase; *Sw*, Switch; *OC*, Open-Circuit; *Des*, Desired; *Al*, Auxiliary Load; *Cl*, Clutch; *Sat*, Saturated; *Act*, Actual

* Corresponding author.
E-mail addresses: snuesch@umich.edu (S. Nüesch), annastef@umich.edu (A.G. Stefanopoulou).

http://dx.doi.org/10.1016/j.conengprac.2016.09.002
0967-0661/

Babajimopoulos, Ortiz-Soto, and Papalambros (2012). In such a configuration fluctuations in desired torque can be compensated using the electric machine while operating the engine at a constant load in the efficient HCCI regime, resulting in additional fuel economy improvements. However, Cairns and Blaxill (2005), Kulzer et al. (2007), Ma et al. (2001), Ortiz-Soto et al. (2012), Delorme et al. (2010), Lawler et al. (2011), and Ahn et al. (2012) all assumed instantaneous combustion mode switches and neglected any influence by the aftertreatment system. As discussed by Nüesch, Gorzelic, Jiang, Sterniak, and Stefanopoulou (2016), such switches are not instantaneous and they incur dynamics and fuel penalties that need to be addressed by the supervisory controller of the HEV.

Combustion mode switches between SI and HCCI need to be accomplished in very short amount of time and with minimum disturbance in torque. However, during a switch operating conditions are neither optimal for SI and HCCI combustion, thereby resulting in penalties in fuel efficiency. Besides fluctuations in torque during the switch, the delays originating from the mode switch dynamics may also impact the engine's torque response. This has been considered by Nüesch and Stefanopoulou (2015) by incorporating the finite state mode switch model from Nüesch et al. (2016) within the loop of the dynamic vehicle simulation and by implementing a supervisory control structure for a SI/HCCI cam switching strategy.

Mild HEVs based on 48 V-systems with relatively small electric machines and batteries are shown to be a cost-efficient way to achieve reasonable improvements in fuel economy (Rick & Sisk, 2015). In this paper a SI/HCCI multimode engine integrated in a 48 V-system with belt-driven integrated starter-generator (ISG) is discussed. The dynamic drive cycle model from Nüesch and Stefanopoulou (2015) is extended by implementing models of electric machine and battery to allow HEV-operation. A part of this research has been presented by Nüesch and Stefanopoulou (2016b) with a focus on emissions aftertreatment. This article expands on that work by comparing four different supervisory control strategies for SI/HCCI mode switching in terms of fuel economy and engine operation. Three of those strategies are rule-based and one represents an equivalent consumption minimization strategy (ECMS).

This article is organized as follows: In Section 2 an overview of the vehicle model is shown, with additional details in the Appendix. In Section 3 the tested supervisory control strategies are presented. Finally, the associated drive cycle results are discussed in Section 4. The second part of this simulation study that accounts for the emission aftertreatment constraints can be found in Nüesch and Stefanopoulou (2016a).

2. Vehicle model

The longitudinal vehicle model was parameterized for a stock Cadillac CTS 2009 with 6-speed manual transmission, a curb mass of 1700 kg, and conventional powertrain with SI combustion engine (Nüesch, Hellström, Jiang, & Stefanopoulou, 1981). Engine cold-start during the FTP75 cycle (approx. first 5 min) is captured by applying a methodology presented by Gao, Conklin, Daw, and Chakravarthy (2010). It is assumed that during this time period a mode switch from SI to HCCI combustion cannot be achieved. The model was developed in MATLAB/Simulink/Stateflow and a detailed model validation with chassis dynamometer measurements can be found in Nüesch (2015). In general the accuracy of the model in terms of drive cycle fuel economy was ±6%. Fig. 1 depicts the block diagram of the vehicle model. Further descriptions of the model can be found in the Appendix.

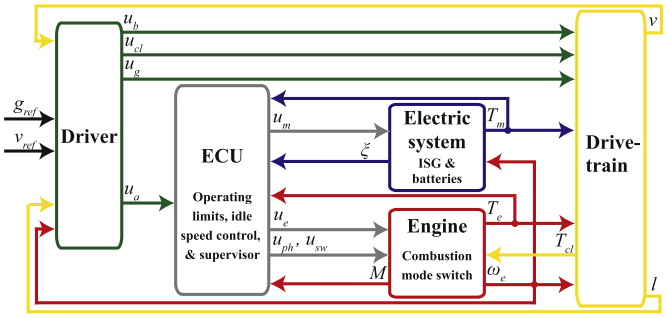

Fig. 1. Block diagram of the vehicle model. For the conventional vehicle the electric system is only used to generate power for the electric auxiliaries.

2.1. Overview and nomenclature

This paper discusses two vehicle configurations. First, the *conventional vehicle* that uses the ISG only as alternator to generate power for the electric auxiliaries without interfering with the SI/HCCI operation. Second, the vehicle denoted *HEV*, which utilizes the ISG's capabilities for torque-assist, regenerative braking, and start/stop. Both vehicles are tested with SI-only as well as with SI/HCCI multimode combustion engine. In case of the HEV, for engine-types, adaptive ECMS is applied to determine the torque split between ISG and engine.

Furthermore, due to the SI/HCCI mode switching dynamics and penalties a supervisory strategy is required to decide when to perform a switch. This decision is not necessarily linked to ECMS and could be solely rule-based. The four tested supervisory strategies for SI/HCCI multimode operation, denoted *Bsl*, *Ext*, *Max*, and *Opt*, represent alternative ways to integrate the mode switching decision into the general HEV torque definition. Due to the number of strategies and the complexity of the system, several variables describing engine torque are used throughout this paper. To help the reader an overview over these variables and the strategies is provided here, before they will be formally introduced later.

The actual torque of the engine plant is denoted T_e. Input to the engine is torque command u_e. The definition of u_e depends on the vehicle configuration. In case of the conventional vehicle, u_e is based on the desired torque of the driver T_{des}. In case of the mild HEV, on the other hand, the optimal engine torque x_T^* is used to determine u_e. Torque variable x_T is the optimization argument within the ECMS. Due to ECMS and torque saturations at the HCCI limits T_e can deviate from T_{des}. The ISG is used to compensate for differences between T_e and $\tilde{T}_e$, representing an ECU-internal variable for the filtered response of T_{des}.

The baseline strategy *Bsl* commands a mode switch based on T_e and T_{des}. Therefore it does not specifically rely on the ISG torque and can be used in both, the conventional vehicle and the HEV. Strategy *Ext* extends residences in HCCI mode by saturating T_e at the limits of the regime while using the ISG to compensate for the difference in torque. The most aggressive strategy *Max* not only extends residences in HCCI, but also moves T_e into the HCCI regime preemptively. In order to do so this strategy relies on the internal ECU-variable T_3, when determining command u_e and initiating the SI-HCCI mode switch. In the rule-based strategies *Ext* and *Max* ECMS and mode switching decision are not connected. This is different in case of optimal strategy *Opt*, where the mode switching decision is integrated within the ECMS optimization.

2.2. Multimode engine

The engine used in this article is a turbocharged 2.0 L I4 multimode engine. Its model is based on steady-state fuel efficiency data for SI and HCCI combustion. The resulting maps are functions of engine torque and speed and can be found in Fig. 2 as well as in

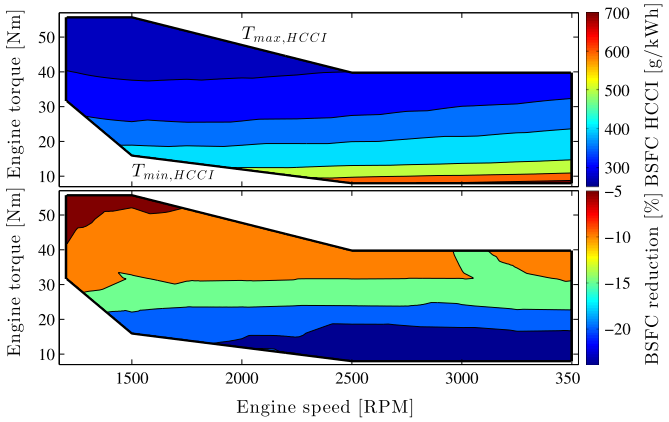

Fig. 2. Steady-state data of the 2.0 L multimode engine in NA HCCI mode. Top: Brake specific fuel consumption of HCCI combustion. Bottom: Fuel efficiency improvement of HCCI over SI.

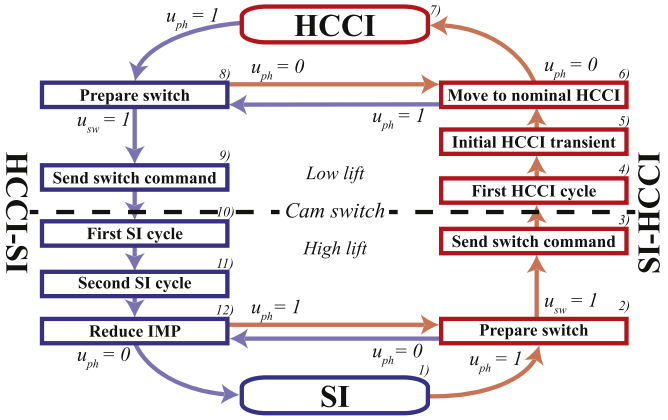

Fig. 3. Combustion mode switch model representing a cam switching strategy. The dashed line illustrates the location of the cam switch.

Nüesch et al. (2016). The maps of the two combustion modes are connected by the combustion mode switch model, also described in Nüesch et al. (2016). This model has been implemented within the dynamic vehicle simulation by Nüesch and Stefanopoulou (2015). It is reiterated here in more detail and extended to allow for HEV-operation.

2.2.1. Operating regime

As discussed above, the feasible operating range of naturally aspirated (NA) HCCI combustion is limited by high pressure rise rates and combustion stability at mid and low loads, respectively. Further limitations originate from allowable NO_x emissions and fuel efficiency. Applying these constraints resulted in the HCCI limits shown in Fig. 2. The function f_R indicates the feasibility of HCCI combustion for specific load/speed conditions:

$$f_R(T, T_{min}, T_{max}) = \begin{cases} \text{HCCI} & T_{min} \le T \le T_{max} \cdots \\ & \text{and } \omega_{min,HCCI} \le \omega_e \le \omega_{max,HCCI} \\ \text{SI} & \text{else.} \end{cases} \quad (1)$$

It is used to evaluate if actual and the desired engine torque, T_e and T_{des}, respectively, lie within the limits of the HCCI regime:

$$R_{act} = f_R(T_e, T_{min,HCCI}, T_{max,HCCI}) \quad (2)$$

$$R_{des} = f_R(T_{des}, T_{min,HCCI}, T_{max,HCCI}). \quad (3)$$

2.2.2. Combustion mode switch

The combustion mode switch model is the core component of the vehicle model. A finite state machine, shown in Fig. 3, is used to describe the mode switch dynamics in a simplified manner. The configuration of the model represents a cam switching strategy in which a two-stage cam switching mechanism is used to transition between the two combustion modes. The model was parameterized using closed-loop mode switch experiments between SI and HCCI at different operating conditions. More on the mode switch control strategy as well as the associated experimental data can be found in Nüesch et al. (2016), Gorzelic et al. (2016), and Gorzelic (2015).

The model distinguishes between 12 mode switch states M, as shown in Fig. 3. Finite state M is the output of the state machine and either SI, HCCI, or one of the intermediate mode switch states. States $M \in (4–9)$ operate under low valve lift conditions, while $M \in (1–3, 10–12)$ are at high lift, with the cam switch in-between. Each intermediate state includes parameters for fuel penalty d_M as well as a residence time Δt_M. The parameters of the finite state model can be found in Table 1. Fuel penalties and residence times are based on closed-loop SI-HCCI and HCCI-SI mode switch experiments. More on determining the mode switch fuel penalties in Gorzelic (2015). Depending on the control inputs and upon passing of the required residence time the state machine progresses to the next state. The model consists of the following two control inputs:

- The input u_{ph} initiates a mode switch (subscript *ph* for cam PHasing). If signal $u_{ph} = 1$, the cams are phased from their regular to the switching position. This process is reversed and the cams moved to their initial location if $u_{ph} = 0$.
- The second signal u_{sw} controls the actual cam switch command (subscript *sw* for cam SWitch). If the cams are in position and $u_{sw} = 1$ the cam switch command is sent. This represents the point-of-no-return during the combustion mode switch.

Table 1
Finite state mode switch model parameters for SI/HCCI cam switching strategy. Fuel penalties are relative to nominal baseline fuel flow in SI or HCCI. Residence times are in seconds or engine cycles. In $M = 2$ the duration is interpolated as a function of current engine load, with shorter durations at the top and longer durations at the bottom HCCI load limit.

State M	Baseline	Fuel penalty d_M (%)	Residence time Δt_M
SI-HCCI			
2	(SI)	6	0.24–0.42 s
3	(SI)	0	1 cyc
4	(HCCI)	14	1 cyc
5	(HCCI)	3	2 cyc
6	(HCCI)	0	3 cyc
HCCI-SI			
8	(HCCI)	4	0.25 s
9	(HCCI)	14	1 cyc
10	(SI)	68	1 cyc
11	(SI)	60	1 cyc
12	(SI)	5	0.25 s

Simulations in which this mode switch model is applied are denoted as *penalized*. Conversely, also results are shown for *instantaneous* mode switches, which do not incur a fuel penalty and involve direct transitions between states $M \in (1, 7)$.

2.2.3. Mode switch scheduling

Exemplary SI-HCCI and HCCI-SI mode switches during a drive cycle simulation are shown in Fig. 4, left and right side, respectively. The presented trajectories belong to a conventional vehicle during the FTP75 drive cycle with penalized mode switches and strategy *Bsl*, which will be described in detail in Section 3.

The supervisory control strategies, described in Section 3, result

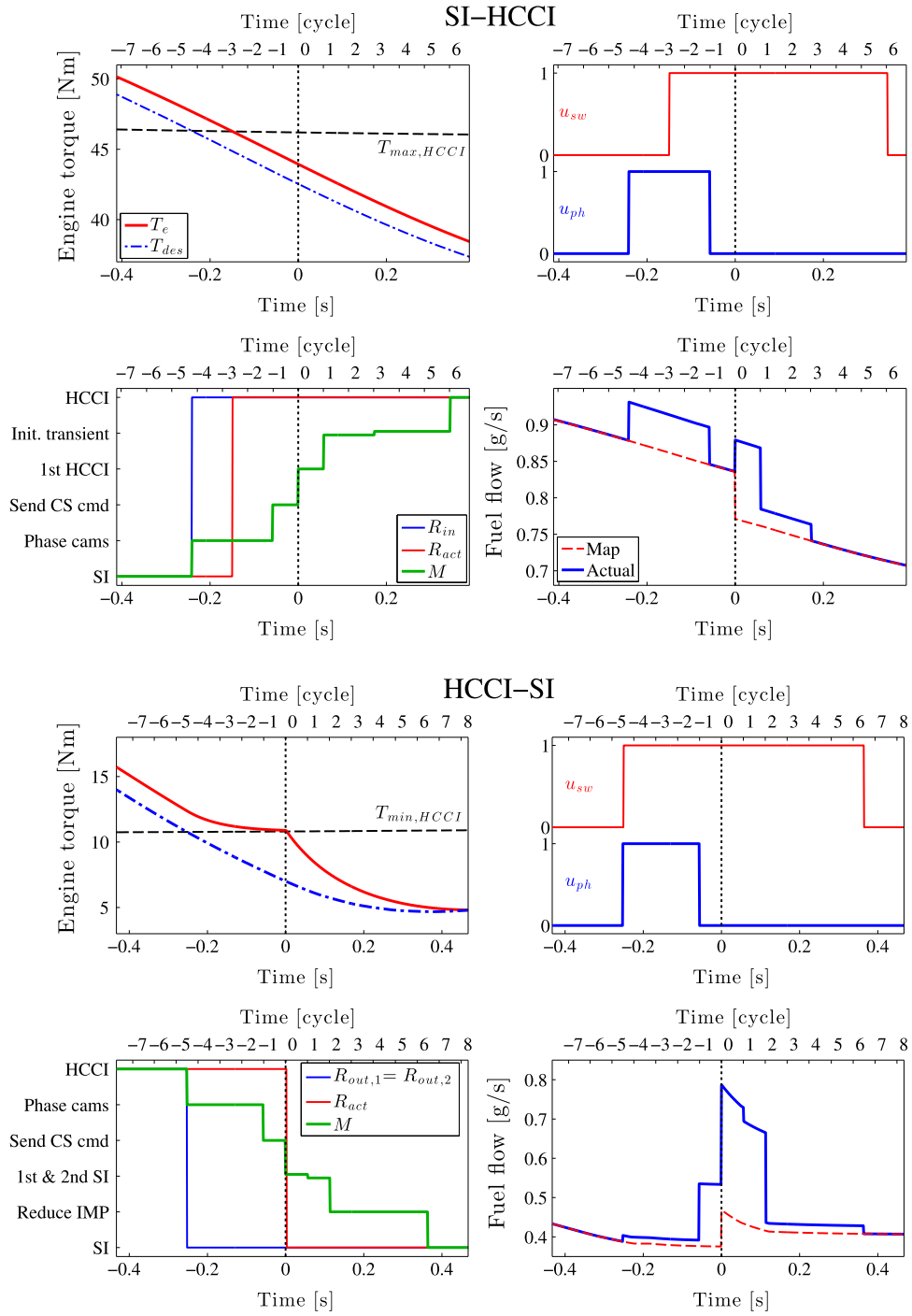

Fig. 4. Exemplary combustion mode switches from SI to HCCI (top) and HCCI to SI (bottom) during simulation of the conventional vehicle, supervisory strategy *Bsl*, and the FTP75 drive cycle. The variables are plotted over time (bottom-axis) and engine cycles (top-axis). Engine speed is 2500 RPM. The finite states $M \in (5, 6)$ are both summarized as *Init. transient*.

in requested operating regimes, denoted R_{in}, R_{act}, $R_{out,1}$, and $R_{out,2}$. Mode switches in SI-HCCI direction are based on R_{act} and R_{in}, while the HCCI-SI direction is determined by $R_{out,1}$ and $R_{out,2}$. These inputs will be mathematically defined in Section 3 and are here only briefly introduced. R_{in} signals that a SI-HCCI mode switch is desired and initializes its preparation. R_{act} determines if the T_e is located within the HCCI regime and a cam switch can be performed. On the other hand, $R_{out,1}$ determines only the preparation of the HCCI-SI mode switch while $R_{out,2}$ is responsible for commanding the actual cam switch. Eqs. (4)–(11) describe how these inputs are translated into appropriate actions u_{ph} and u_{sw} during the mode switch, depending on the current combustion mode M.

- In SI, $M = 1$, the input R_{in} initializes the mode switch. R_{in} represents the combustion mode preferred by the supervisory strategy. In case of Fig. 4 (left) R_{in} is triggered by the desired engine torque T_{des} entering the HCCI regime at $t = -0.24$ s:

$$u_{ph} = \begin{cases} 1 & R_{in} = \text{HCCI} \\ 0 & \text{else} \end{cases} \tag{4}$$

$$u_{sw} = 0 \tag{5}$$

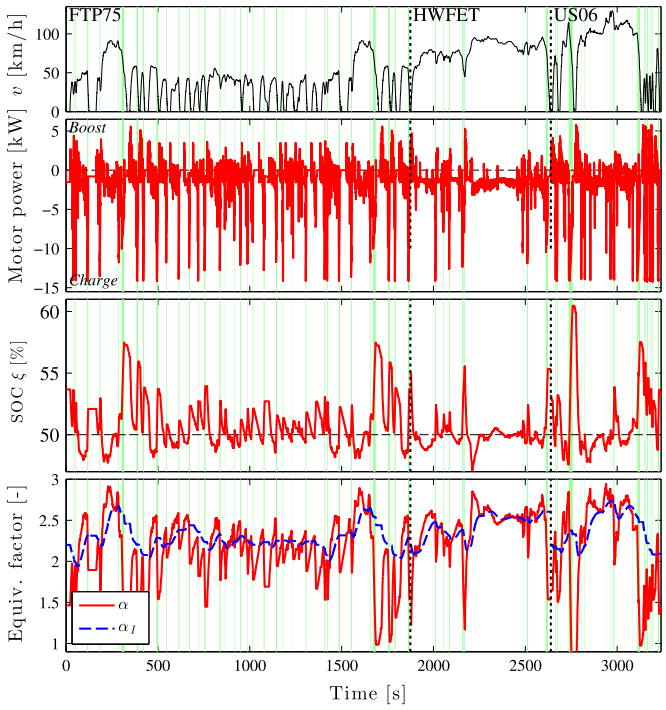

Fig. 5. Trajectories of the SI-only HEV during the simulation of the three drive cycles. Top: Velocity v. Second: Motor power P_m. Third: Battery SOC ξ. Bottom: Equivalence factor α (solid red) and its integral part α_I (dashed blue). Time periods allowing for regenerative braking are highlighted in green. (For interpretation of the references to color in this figure caption, the reader is referred to the web version of this paper.)

- The finite state machine progresses to state $M = 2$. The cams are being phased to a position ready to switch to low lift, controlled by R_{in}. The cam switch command is sent as soon as the current engine conditions R_{act} allow, as shown in Fig. 4 (top) at $t = -1$ cycle. The actual cam switch occurs one engine cycle later:

$$u_{ph} = \begin{cases} 0 & R_{act} = SI \text{ and } R_{in} = SI \\ 1 & \text{else} \end{cases} \tag{6}$$

$$u_{sw} = \begin{cases} 1 & R_{act} = \text{HCCI and } R_{in} = \text{HCCI} \\ 0 & \text{else} \end{cases} \tag{7}$$

- In HCCI, $M = 7$, the cams are prepared for the switch back to SI if demanded by any of the inputs $R_{out,1}$ or $R_{out,2}$. In case of Fig. 4 (bottom) this is due to T_{des} exiting the HCCI regime at $t = -0.25$ s:

$$u_{ph} = \begin{cases} 1 & R_{out,1} = \text{SI or } R_{out,2} = \text{SI} \\ 0 & \text{else} \end{cases} \tag{8}$$

$$u_{sw} = 0 \tag{9}$$

- Similar to the other mode switch direction in $M = 8$ the cams remain in prepared conditions until both $R_{out,1}$ and $R_{out,2}$ demand SI mode:

$$u_{ph} = \begin{cases} 0 & R_{out,1} = \text{HCCI and } R_{out,2} = \text{HCCI} \\ 1 & \text{else} \end{cases} \tag{10}$$

$$u_{sw} = \begin{cases} 1 & R_{out,1} = SI \text{ and } R_{out,2} = SI \\ 0 & \text{else} \end{cases} \tag{11}$$

- Upon entering high lift conditions, $M \in (10, 11)$, the engine will be operated rich to enable the TWC to reduce the increased levels NO_x, resulting in relatively high fuel efficiency penalties during the first two engine cycles in SI mode. After this phase it can be decided to operate at stoichiometry, $M \in (12, 1)$, or alternatively initiate another switch to HCCI, as described by (4) and (5).

2.2.4. Engine torque command

The variable u_e represents the engine torque command. While in SI mode, specifically at high cam lift conditions (lower half of Fig. 3), the entire load range is available and the torque by the engine can be delivered unconditionally. However, in HCCI, specifically as long as the cams are in low lift (upper half of Fig. 3), the torque is constrained by HCCI's operating limits. Therefore the command to the engine needs to be saturated, which is emulated by function f_{sat}:

$$f_{sat}(T, M) = \begin{cases} T_{max,HCCI} & T \geq T_{max,HCCI} \text{ and } M \in (4\text{–}9) \\ T_{min,HCCI} & T \leq T_{min,HCCI} \text{ and } M \in (4\text{–}9) \\ T & \text{else.} \end{cases} \tag{12}$$

In case of the conventional vehicle u_e is based on the desired load T_{des}:

$$u_e = f_{sat}(T_{des}, M). \tag{13}$$

Conversely, in case of the HEV u_e is determined by the optimum engine torque x_T^*:

$$u_e = f_{sat}(x_T^*, M). \tag{14}$$

x_T^* is the result of the ECMS, as defined by (18) in Section 2.4.

2.3. Integrated starter-generator (ISG)

A model for a belt-driven ISG based on first-order dynamics is used to evaluate potential synergies between multimode combustion and mild hybridization. The ISG with a maximum continuous power of 5 kW boost and 14 kW regeneration represents a small e-machine as seen in upcoming 48 V systems. A belt-ratio of $\gamma_b = 2.5$ is used to connect engine and ISG. In the conventional vehicle the ISG simply operates as alternator to deliver power for electric auxiliaries. In the HEV, the ISG is additionally used for start/stop operation, torque assist, and regenerative braking. Regenerative braking is activated if the brake pedal u_b is pressed, ordering the ISG to generate as much power as possible while matching the brake demand. The regenerative braking events during the three drive cycles are highlighted in Fig. 5. More on the ISG model and the electric auxiliaries can be found in Appendix A.2. Details on the ISG hardware can be found in Kelly, Scanes, and Bloore (2014).

The optimal torque-split between engine and ISG is computed by the ECMS, described in Section 2.4. Due to this optimization in general $u_e \neq T_{des}$, resulting in torque gaps which need to be filled by the ISG. It would be possible to use the raw desired torque T_{des} to determine the ISG torque required to bridge those gaps. The ISG's time constant is an order of magnitude faster than engine time constant τ_e. This would allow to track the driver's demand more accurately than the conventional vehicle. However, the goal here is to compare the performance of the HEV powertrain to the conventional vehicle without changing the combined response of engine and ISG. For that reason the time constant of the engine is used to filter the desired driver torque T_{des} and to compute $\tilde{T}_e$, which represents the virtual engine torque the driver expects from the conventional vehicle:

$$\dot{\tilde{T}}_e = \frac{1}{\tau_e}(T_{des} - \tilde{T}_e). \tag{15}$$

The ISG is used to compensate for the gap between virtual and actual engine torque, $\tilde{T}_e$ and T_e, respectively. The associated torque

command to the ISG $u_{m,c}$ is defined as:

$$u_{m,c} = \frac{1}{\gamma_b}(\tilde{T}_e - T_e). \tag{16}$$

This definition also compensates for over torque gaps, e.g., due to torque saturations at the limits of the HCCI regime (14).

2.4. Adaptive ECMS

The equivalent consumption minimization strategy (ECMS) is a widely applied method to achieve in real-time the close-to-optimal fuel economy of a HEV while maintaining battery SOC (Guzzella & Sciarretta, 2007). At each time step the torque split between engine and ISG is determined which minimizes the instantaneous equivalent power consumption:

$$J(x_T) = P_f(x_T) + \alpha \cdot P_c(x_T) \tag{17}$$

$$x_T^* = \underset{x_T \in X}{\operatorname{argmin}} J(x_T). \tag{18}$$

The argument of the minimization is engine torque x_T, constrained to the space of admissible controls X, which is mainly based on the limits of the current combustion mode M, SI or HCCI, and the limits of the ISG:

$$X = \{x_T | T_{min}(M) \le x_T \le T_{max}(M) \text{ and } \dots \tag{19}$$

$$T_{m,min} \le \hat{T}_m(x_T) \le T_{m,max}\}. \tag{20}$$

$P_f(x_T)$ and $P_c(x_T)$ are the power released by the burned fuel and by the battery cells, respectively, as a function of engine torque. Co-state α represents the equivalence factor, used to compare the two power sources and thereby maintaining SOC close to its reference.

The commanded engine torque u_e is generally equal to x_T. Exceptions are idle and when the engine torque is saturated at the limits of the corresponding combustion mode:

$$u_e = f(x_T) \tag{21}$$

$$u_e \approx x_T. \tag{22}$$

2.4.1. Equivalence factor

Different alternatives are available on how to determine the equivalence factor α. Onori and Serrao (2011) compare several adaptive approaches, in which α is defined as a function of battery SOC ξ. In this paper the approach by Chasse, Corde, Del Mastro, and Perez (2010) is used, in which a PI controller modifies α to track a reference SOC ξ_{ref}, in this case $\xi_{ref} = 50\%$:

$$\alpha = K_P \cdot (\xi_{ref} - \xi) + \underbrace{K_I \cdot \int (\xi_{ref} - \xi) dt}_{\alpha_I}. \tag{23}$$

with controller gains $K_p = 20$ and $K_I = 0.5$ obtained by manual tuning. To ensure the final SOC to be close to the initial SOC the drive cycles were simulated repeatedly, similar to Borhan et al. (2012). The initial SOC for FTP75, HWFET, and US06 are 53.7%, 55.2%, and 53.3%, respectively, and the difference between final and initial SOC was for all cases smaller than 0.01%. The drive cycle trajectories of motor power $P_m = T_m \cdot \omega_m$, equivalence factor, and SOC are plotted in Fig. 5.

2.4.2. Computation of equivalent power

The fuel power is computed using the steady-state maps of the two combustion modes:

$$P_f(x_T) = H_f \cdot \dot{m}_f(x_T, M) \tag{24}$$

$$\dot{m}_f(x_T, M) = \begin{cases} f_{SI}(x_T, \omega_e) & M = \text{SI} \\ f_{HCCI}(x_T, \omega_e) & M = \text{HCCI} \end{cases} \tag{25}$$

with lower heating value of gasoline H_f. The gap between desired torque T_{des} and engine torque argument x_T needs to be compensated by the ISG. The resulting motor torque argument $\hat{T}_m(x_T)$ is constrained by the limits of the ISG via space X and takes into account the load demanded by the electric auxiliaries $u_{m,al}$. Find more on $u_{m,al}$ in Appendix A.2:

$$\hat{T}_m(x_T) = u_{m,al} + \frac{1}{\gamma_b}(T_{des} - x_T) \tag{26}$$

Eqs. (A.2)–(A.7) from Section A.3 of the Appendix are applied to compute current in the battery cells $\hat{I}_c(x_T)$ from $\hat{T}_m(x_T)$. Ultimately the power released by the battery cells $P_c(x_T)$ follows as:

$$P_c(x_T) = n_p \cdot n_s \cdot \hat{I}_c(x_T) \cdot U_{OC}(\xi) \tag{27}$$

with the number of battery cells in series and in parallel, n_p and n_s, respectively, and open-circuit voltage U_{OC} as a function of SOC ξ.

3. Supervisory control strategies

In this section four supervisory control strategies for SI/HCCI mode switching are described. The first strategy is demonstrated for both, conventional vehicle and mild HEV. The remaining three strategies rely on the torque assist by the ISG. An exemplary residence in HCCI mode is shown in Fig. 6 to compare the four supervisors. The jerky behavior of engine torque T_e results from the discretization of the ECMS. The block diagrams of the supervisors are depicted in Fig. 7.

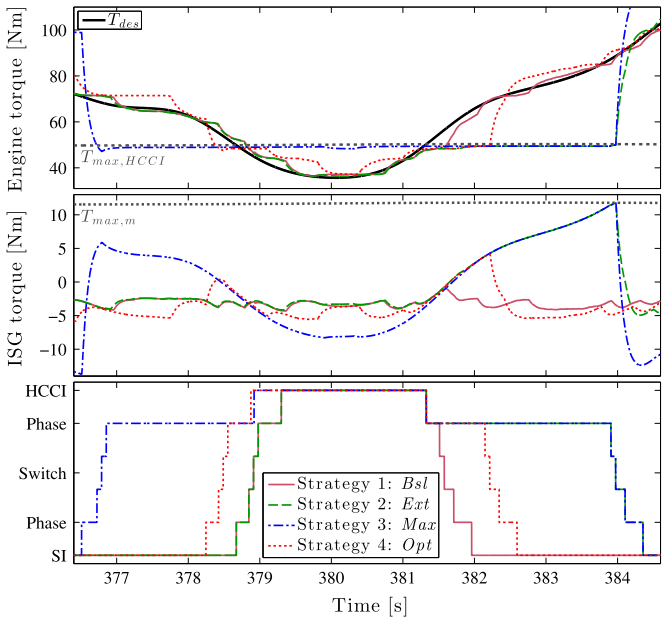

Fig. 6. Exemplary residence in HCCI mode during the HWFET cycle to compare the four supervisory strategies *Bsl* (solid brown), *Ext* (dashed green), *Max* (dash-dotted blue), and *Opt* (dotted red). Top: Engine torque with desired torque T_{des} (solid black). Middle: ISG torque T_m. Bottom: Combustion mode M. (For interpretation of the references to color in this figure caption, the reader is referred to the web version of this paper.)

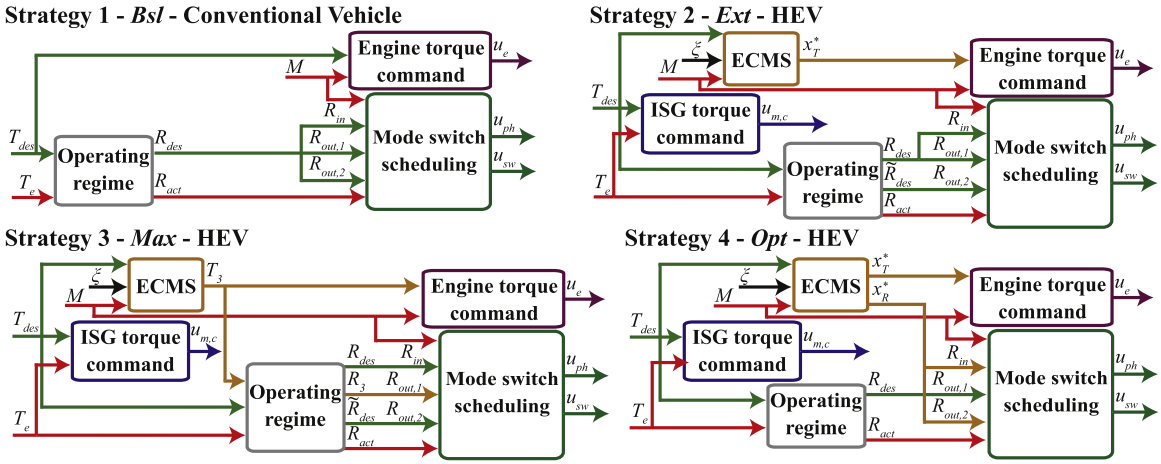

Fig. 7. Block diagrams of the four supervisory control strategies.

3.1. Strategy 1: Baseline (Bsl)

The first supervisory control strategy *Bsl* has been described by Nüesch and Stefanopoulou (2015). It prepares the SI-HCCI mode switch as soon as T_{des} enters the HCCI regime, as can be seen in Fig. 6 at $t = 378.6$ s. The cams are switched to low-lift as soon as the valves reached their switching positions and T_e enters the HCCI regime. Conversely, in the HCCI-SI direction the mode switch is prepared when T_{des} exits the HCCI regime, in Fig. 6 at $t = 381.3$ s. If by the time the valves reach their switching position T_{des} still lies outside the HCCI boundaries, the cam switch to high-lift is initiated. Therefore the following variables are all equal:

$$R_{in} = R_{out,1} = R_{out,2} = R_{des}. \tag{28}$$

As can be seen, when applied in the mild HEV this strategy does not attempt to extend the residence time in HCCI mode. However, additional benefits in fuel economy are possible, since ECMS exploits high efficiency areas within the HCCI regime.

As described by Nüesch and Stefanopoulou (2015) $T_{min,HCCI}$ and $T_{max,HCCI}$ could be altered to modify $R_{out,2}$ with the goal to trade-off drivability with fuel economy. Alternatively, as discussed by Nüesch, Sterniak, Jiang, and Stefanopoulou (2015), prediction could be used to improve the controller's performance by anticipating upcoming crossings of the HCCI limits.

Depending on the applied vehicle, conventional or hybrid, the commanded engine load u_e is determined by (13) or (14), respectively.

3.2. Strategy 2: extended stay (Ext)

The second supervisory strategy *Ext* can be realized in a mild HEV with multimode engine. It aims to improve fuel economy by extending the residence time in HCCI while reducing the number of mode switches, by relying on the ISG to delay the HCCI exit as much as possible. The ISG is used to create a virtual HCCI regime, which is composed of the actual HCCI limits and the ISG's torque range:

$$\tilde{T}_{max,HCCI} = T_{max,HCCI} + \gamma_b \cdot (T_{max,m} - u_{m,al}) \tag{29}$$

$$\tilde{T}_{min,HCCI} = T_{min,HCCI} + \gamma_b \cdot (T_{min,m} - u_{m,al}). \tag{30}$$

The virtual HCCI regime accounts for the ISG torque required to power the electric auxiliaries $u_{m,al}$. As in strategy *Bsl* a mode switch from SI to HCCI is commanded if T_{des} enters the HCCI regime. However, in case of strategy *Ext*, if T_{des} exits the actual HCCI regime, the engine torque command u_e saturates at the HCCI limits. Concurrently the ISG is used to bridge the gap between engine torque T_e and desired torque T_{des}. At the same time the valves are phased to their target switching position. Therefore, once the desired torque exits the virtual HCCI regime, the cam switch command can be sent and the HCCI-SI mode switch executed immediately, as in Fig. 6 at $t = 384$ s:

$$R_{in} = R_{out,1} = R_{des} = f_R(T_{des}, T_{min,HCCI}, T_{max,HCCI}) \tag{31}$$

$$R_{out,2} = \tilde{R}_{des} = f_R(T_{des}, \tilde{T}_{min,HCCI}, \tilde{T}_{max,HCCI,m}) \tag{32}$$

Remaining in a prepared state while still being in the virtual HCCI regime has the advantage of a minimum delay in total propulsion torque once the driver desires to accelerate. A potential disadvantage, on the other hand, is that this prepared state involves valve timings different from their nominal HCCI condition, which might result in a small reduction in engine efficiency.

As in the SI-only case, with strategy *Ext* the torque command to the engine u_e is determined by ECMS and x_T^* (14).

3.3. Strategy 3: maximum stay (Max)

The strategy above is modified to prolong the residence time in the HCCI regime even further. Similar to *Ext*, strategy *Max* uses the ISG to delay switches from HCCI to SI. However, in addition *Max* also shifts the engine load to the HCCI regime preemptively, as shown in Fig. 6 at $t = 376.7$ s. If T_{des} enters a band above and below the actual HCCI regime, the load is forced into the regime. The lower band was chosen between $T_{min,HCCI}$ and 0 N m. The width of the upper band is determined by parameter $\Delta T \in \left(0\text{ N m}, \gamma_b \cdot (T_{max,m} - u_{m,al})\right)$. The smaller the value of ΔT the more aggressive the strategy. Strategy *Ext* can be implemented by selecting $\Delta T = 0$ N m. The optimal value of ΔT depends on the drive cycle. Here $\Delta T = 15$ N m was chosen as a reasonable value without any prior optimization. As reference, at 2000 RPM the maximum torque of the ISG at the driveshaft is 24 N m:

$$T_3 = \begin{cases} T_{min,HCCI} & 0 < T_{des} < T_{min,HCCI} \\ T_{max,HCCI} & T_{max,HCCI} < T_{des} < \tilde{T}_{max,HCCI} - \Delta T \\ x_T^* & \text{else.} \end{cases} \tag{33}$$

The mode switch in HCCI-SI direction is controlled in the same fashion as in strategy *Ext*:

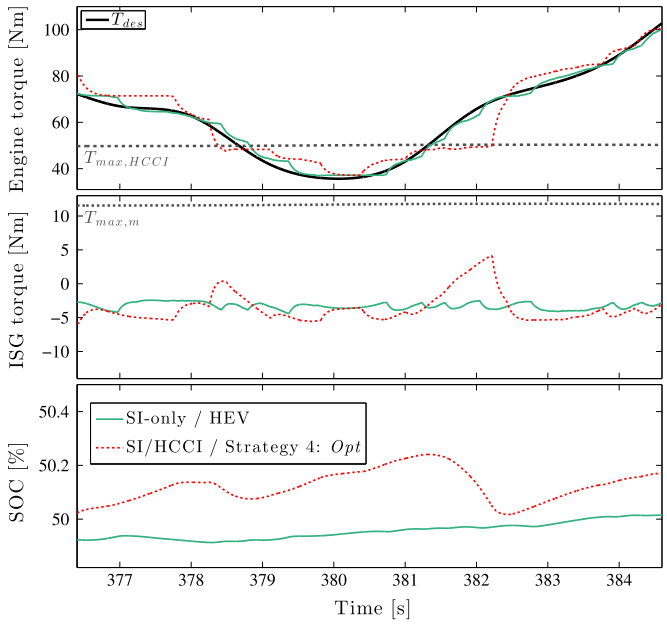

Fig. 8. Exemplary residence in HCCI mode during the HWFET cycle to compare the SI-only HEV (solid green) with the SI/HCCI HEV applying the fourth supervisory strategy *Opt* (dotted red). Top: Engine torque with desired torque T_{des} (solid black). Middle: ISG torque T_m. Bottom: SOC ξ. (For interpretation of the references to color in this figure caption, the reader is referred to the web version of this paper.)

$$R_{in} = R_3 = f_R(T_3, T_{min,HCCI}, T_{max,HCCI}) \tag{34}$$

$$R_{out,1} = R_{des} = f_R(T_{des}, T_{min,HCCI}, T_{max,HCCI}) \tag{35}$$

$$R_{out,2} = \tilde{R}_{des} = f_R(T_{des}, \tilde{T}_{min,HCCI}, \tilde{T}_{max,HCCI}). \tag{36}$$

Since this strategy requires to modify the engine torque to move to the regime, here the torque command u_e is based on T_3 instead of x_T^*:

$$u_e = f_{sat}(T_3, M). \tag{37}$$

3.4. Strategy 4: optimal stay (Opt)

Instead of making a rule-based decision about when to enter or exit HCCI mode, as done in the previous supervisors, strategy *Opt* integrates the decision into the ECMS control structure.

Eq. (18) is replaced with the following minimization to determine the optimal torque split x_T^* together with the currently optimal combustion mode x_R^*:

$$J(x_T, x_R) = P_f(x_T, x_R) + \alpha \cdot P_c(x_T) \tag{38}$$

$$(x_T^*, x_R^*) = \arg \min_{x_T \in X, x_R \in \{\text{SI,HCCI}\}} J(x_T, x_R) \tag{39}$$

with the space of admissible controls X now a function of x_R:

$$X(x_R) = \{x_T | T_{min}(x_R) \le x_T \le T_{max}(x_R) \text{ and } \ldots \tag{40}$$

$$T_{m,min} \le \hat{T}_m(x_T) \le T_{m,max}\}. \tag{41}$$

The computation of the fuel power is modified as well to be incorporated with the fuel penalties of the mode switches:

$$P_f(x_T, x_R) = H_f \cdot \dot{m}_f(x_T, x_R, M) \tag{42}$$

$$\dot{m}_f(x_T, \text{SI}, M) = \begin{cases} f_{SI}(x_T, \omega_e) & M = \text{SI} \\ f_{SI}(x_T, \omega_e) \cdot (1 + d_2) & M = \text{HCCI} \end{cases} \tag{43}$$

$$\dot{m}_f(x_T, \text{HCCI}, M) = \begin{cases} f_{HCCI}(x_T, \omega_e) & M = \text{HCCI} \\ f_{HCCI}(x_T, \omega_e) \cdot (1 + d_1) & M = \text{SI} \end{cases} \tag{44}$$

Eq. (43) is used to compute the fuel consumption of remaining in SI and switching to SI from HCCI mode, (44) vice versa. The variables d_1 and d_2 represent the total penalties in terms of fuel flow for the SI-HCCI and HCCI-SI mode switches, respectively, and are calculated as follows:

$$d_1 = \frac{1}{\tau_1} \cdot \left(\sum_{M \in (2-6)} d_M \cdot \Delta t_M \right) \tag{45}$$

$$d_2 = \frac{1}{\tau_2} \cdot \left(\sum_{M \in (8-12)} d_M \cdot \Delta t_M \right). \tag{46}$$

As can be seen these penalties represent the total fuel penalty divided by tuning parameters τ_1 and τ_2. These parameters can be interpreted as the average duration to the next mode switch. Larger values of τ_1 and τ_2 lead to encouragement and smaller values prevent mode switching. Their optimal choice depends on the applied drive cycle, but it was seen that their influence on the fuel economy result is overall limited. Here reasonable values $\tau_1 = 1$ s and $\tau_2 = 6$ s were chosen without any optimization.

Therefore, rather than from any load commands, the switches to and from HCCI are ultimately determined by the ECMS x_R^*. In Fig. 6 the SI-HCCI and HCCI-SI switches can be seen at $t = 378.4$ s and $t = 382.3$ s, respectively. In addition, similar to strategies *Ext* and *Max* the HCCI-SI mode switch is prepared if T_{des} leaves the HCCI regime:

$$R_{in} = R_{out,2} = x_R^* \tag{47}$$

$$R_{out,1} = f_R(T_{des}, T_{min,HCCI}, T_{max,HCCI}). \tag{48}$$

Similar to strategies *Bsl* and *Ext* the engine torque command u_e is computed by (14).

A comparison between the SI-only HEV and the SI/HCCI HEV applying strategy *Opt* is shown in Fig. 8. It depicts the same exemplary residence in HCCI as Fig. 6. It can be seen how strategy *Opt* utilizes battery SOC to extend the residence time in HCCI mode.

4. Drive cycle results

The drive cycle results are discussed in the following section, first in terms of general characteristics, then focused on the four supervisory strategies and associated fuel economy.

4.1. Drive cycle characteristics

The visitation frequencies of different engine load/speed conditions during the three drive cycles are shown in Fig. 9 for the conventional vehicle applying supervisory strategy *Bsl* and the HEV using strategy *Opt*. As can be seen, ECMS in SI mode reduces high load operation by shifting the operating conditions to lower

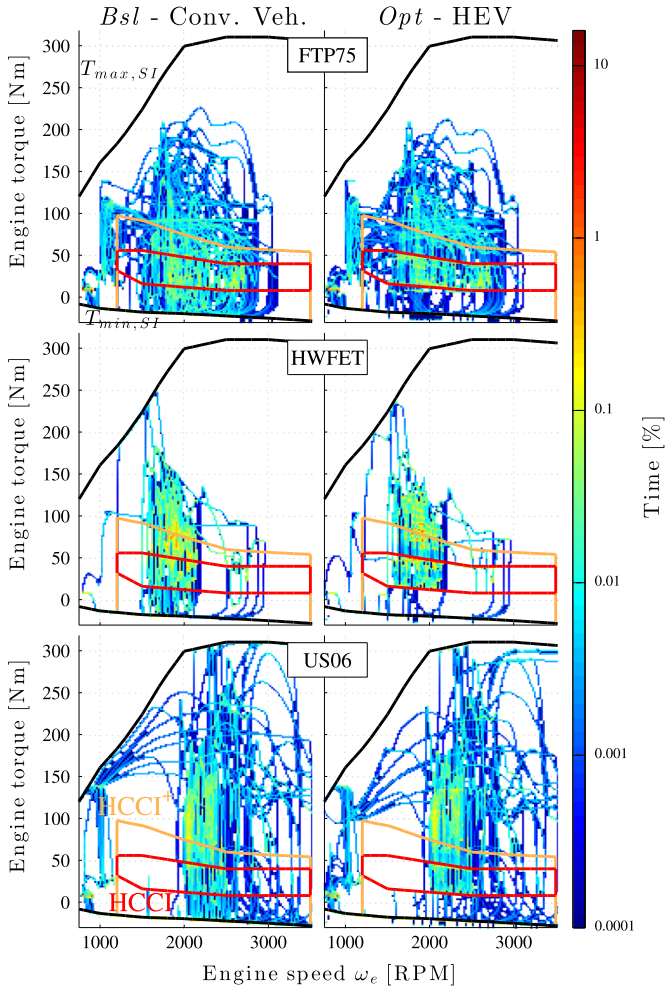

Fig. 9. Operating regimes and load/speed visitation frequencies of the multimode engine. Top: FTP75. Middle: HWFET. Bottom: US06. Compared are the conventional vehicle applying strategy *Bsl* (left) with the mild HEV using strategy *Opt* (right). Limits of SI and HCCI in black and red, respectively and HCCI regime extended by ISG (HCCI$^+$) in orange. (For interpretation of the references to color in this figure caption, the reader is referred to the web version of this paper.)

loads. Furthermore, the plots show the effect of the mode switching supervisors and strategy *Opt* in particular. The supervisory strategies shift frequently visited operating conditions from the extended HCCI regime inside the HCCI regime. Thereby they create bands above and below the HCCI regime where the engine barely operates. At the same time, in case of the HEV the distribution of visitations within the HCCI regime is less homogeneous and more concentrated at the load boundaries compared to the conventional vehicle. The reason is short excursions of T_{des} from the HCCI regime which are being compensated for by the ISG while the engine torque is held close to the boundaries.

Table 2
Drive cycle characteristics.

Characteristic	FTP75	HWFET	US06
Fuel economy benefit			
From start/stop	4.5%	0.11%	0.82%
From start/stop & ECMS	8.7%	1.8%	3.8%
Mean desired torque	22 N m	62 N m	70 N m
Mean regenerative braking energy	66 J/m	14 J/m	52 J/m
Fraction of time desired torque spent			
In HCCI regime	19.8%	20.4%	7.3%
In extended HCCI regime	45.8%	63.6%	31.0%

General characteristics of the three drive cycles are listed in Table 2. As can be seen in Fig. 5, the FTP75 velocity profile incorporates substantially more time spent at vehicle standstill than the other two drive cycles. This relates directly to the high fuel savings of 4.5% if start/stop operation is applied. The associated result for the HWFET and US06 is significantly smaller with values below 1%. In addition to significant vehicle standstill the FTP75 drive cycle also exhibits generally lower velocities than the HWFET and US06 as well as less aggressive accelerations than the US06. The three properties are the reason, why the FTP75 exhibits a low desired torque, averaged over time, of 22 N m. This directly relates to the distribution of T_{des}, which spends about 20% of time in the HCCI regime during the FTP75 and the HWFET and only 7% during the US06. If the HCCI regime is extended by the ISG all those numbers more than double to 46%, 64%, and 31% for the FTP75, HWFET, and US06, respectively. The effect is especially strong for the HWFET since its torque distribution is highly concentrated above the HCCI regime at around 70–80 N m, as can also be seen in Fig. 9. In case of the US06 cycle the time spent in the extended HCCI regime is significantly larger than the time spent in the regular regime. However, with only 31% of time it is still relatively low. In contrast to the other drive cycles, the US06 cycle's region of highly visited engine conditions lies at very high torques beyond the extended HCCI regime.

Finally, a large difference between the drive cycles is the amount of energy harvested with regenerative braking. This difference can be seen qualitatively in Fig. 5 and quantitatively by computing the average energy regenerated per distance travelled. As can be seen, the FTP75 cycle with 66 J/m achieves the highest amount of regeneration and the HWFET, with only a handful braking events and 14 J/m the lowest.

The gains due to start/stop operation together with the available battery energy from regenerative braking directly relate to the fuel economy benefit of the mild HEV with SI-only combustion. Here the FTP75 results in 8.7% fuel economy improvement, half of which is due to start/stop. With less battery energy available to reduce the engine load and fewer start/stop events the US06 results in 3.8% improvement. Finally, the gains during the HWFET are even lower with 1.8%, due to virtually no start/stop operation and almost negligible regeneration.

4.2. Fuel economy benefits from multimode combustion

In the following section the fuel economy results for the three drive cycles, shown in Fig. 10, are discussed. It is distinguished between the penalized mode switch model and instantaneous mode switches. The influence of mode switch penalties in case of the conventional vehicle has been discussed in detail in Nüesch et al. (2016). Here it is focused on the effect of hybridization its synergy with the different supervisory strategies.

In case of the HEV and the FTP75 cycle all four supervisory control strategies lead to noticeable improvements in fuel economy. Strategy *Bsl*, however, does not benefit from the hybridization. Its associated relative improvements of 3.0% and 2.0% for instantaneous and penalized mode switches, respectively, are very similar to the ones seen with the conventional vehicle. This is not surprising since strategy *Bsl* does not specifically integrate HCCI operation into the control strategy. On the other hand, strategies *Ext*, *Max*, and *Opt* result in improvements over the SI-only HEV of approximately 5.7% and 4.2% for instantaneous and penalized mode switches, respectively. The performance of the three supervisors is relatively similar in case of the FTP75, all being able to take advantage of the synergy between SI/HCCI multimode operation and the torque assist from the ISG, which allows longer residence time in HCCI combustion while performing fewer fuel-expensive mode switches. Meanwhile, the optimal strategy *Opt*

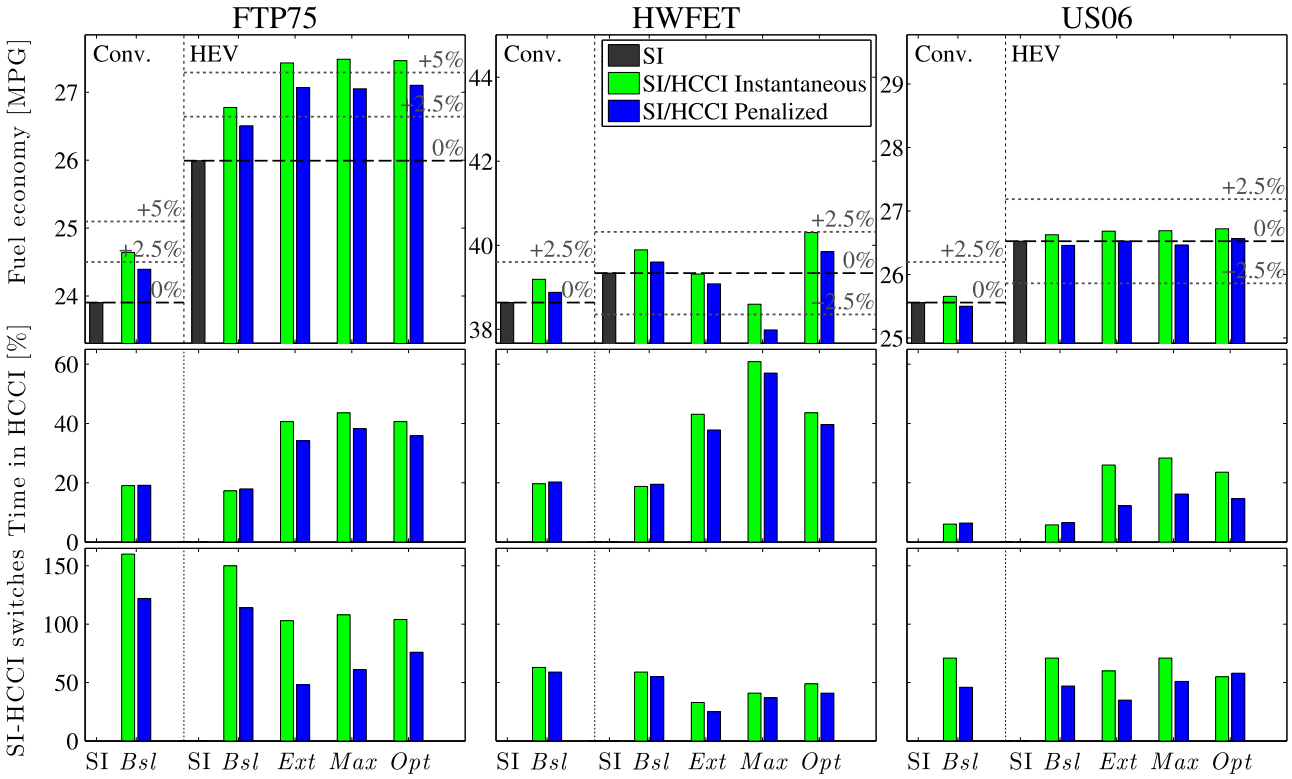

Fig. 10. Drive cycle results assuming an ideal aftertreatment system, which does not require any depletion. Results for FTP75 (left column), HWFET (center column), and US06 (right column) cycles. Plotted are fuel economy (top row), fraction of time spent in HCCI combustion (center row), and number of cam switches from SI to HCCI (bottom row). Conventional vehicle (bars on the left) and mild HEV (bars on the right) with results shown for the SI-only engine (black bars) as well as the SI/HCCI multimode engine applying the four supervisory strategies. Mode switches are assumed instantaneous (green bars) and penalized (blue bars). (For interpretation of the references to color in this figure caption, the reader is referred to the web version of this paper.)

performs only marginally better than *Ext* and *Max*. As discussed above and shown in Fig. 5 the FTP75 drive cycle results in a desired load which is evenly distributed within the extended HCCI regime, with residences in HCCI being regularly interrupted by regenerative braking events. Therefore the HCCI operation does not significantly affect the battery's SOC and it can be concluded that a simple mode switch supervisory strategy is sufficient to achieve high fuel economy benefits from HCCI.

The fuel economy results for the HWFET, however, show a different pattern. Here the optimal strategy *Opt* clearly shows the best performance and again higher relative improvements than strategy *Bsl* and the conventional vehicle. Noticeably, strategies *Ext* and *Max* result in reductions in fuel economy, despite 40–60% of time spent in HCCI mode. As seen above, for a majority of the HWFET cycle the cruise condition lies concentrated right above the HCCI regime. A large amount of electric power is required to shift the engine load down to HCCI for extended periods of time. At the same time opportunities to charge the battery are very sparse. This leads to the poor performance of strategies *Ext* and *Max*. Supervisory strategy *Opt* resolves this issue by returning to SI if at a certain SOC the fuel economy benefits of HCCI are lower than the required battery power to remain in the regime.

Finally, the results for the US06 drive cycle show barely any improvement from using HCCI combustion. With the ISG's torque-assist, penalized mode switches, and strategies *Ext*, *Max*, and *Opt* the total residence time in the HCCI regime doubles compared to the conventional vehicle, from 6% to 14%. This is, however, still small, leading to very limited improvements even when assuming instantaneous mode switches. The residence time in HCCI per cam switch is short as well, resulting in a larger impact of the mode switch penalties. The reason for this low visitation time in the HCCI regime is the fact that a majority of the engine's operating conditions during the US06 cycle are located at relatively high loads. There they too are not within reach of the ISG and cannot be consistently shifted to the HCCI regime. However, strategy *Opt* still achieves at least a neutral fuel economy, in contrast to the negative results shown by the other strategies and by the conventional vehicle.

In general, it can be concluded that two effects are required to successfully exploit the synergies between torque assist in a mild HEV and multimode combustion. First, regular regeneration events and therefore large quantities of available battery energy are required to allow to shift the engine operation into the HCCI regime for significant amounts of time. The consequence of a lack of such events was seen in case of the HWFET, where the SOC-constraint required switches back to SI mode even though a stay in HCCI would have been possible. Second, due to the ISG's limited torque the desired engine load is required to often lie close to the HCCI regime. Otherwise, as seen in case of the US06 cycle, the beneficial HCCI regime cannot be exploited.

In addition, it can be seen that the characteristics of the drive cycle and the associated distribution in desired torque are determined, if SOC represents an important constraint for the SI/HCCI mode switching decision. If the driver's load requirement is located around the extended HCCI regime, including significant residence time at very low loads as seen in the FTP75, the ECMS uses the ISG equally for torque assist and charging. Therefore the SOC does not need to be specifically considered during the mode switch decisions to achieve high fuel economy improvements. However, if the driver continuously requires loads which are located slightly above the HCCI regime, as seen in the HWFET, the ISG is preferably used as torque-assist to compensate for short excursions from the HCCI regime to higher loads. This leads to a significant reduction in SOC, which needs to be considered in the

mode switching decision. Finally, if the average load demand is so high that a small ISG cannot shift it to the HCCI regime, HCCI combustion cannot be used for a significant amount of time anyway, therefore removing any significance of SOC on the mode switch decision.

5. Conclusion

A model of a mild HEV, controlled with ECMS, is combined with a SI/HCCI multimode engine. Four supervisory mode switching control strategies are discussed. The baseline strategy does not utilize torque assist for HCCI operation. Two rule-based strategies extend and maximize the residence time in HCCI without taking into account the battery's SOC. Finally, the optimal strategy incorporates the mode switching decision and associated penalties into the ECMS. The strategies are analyzed in terms of fuel economy benefits and synergies over the FTP75, HWFET, and US06 drive cycles. It is shown that the FTP75 drive cycle, which exhibits a low average load demand and a high number of regenerative braking events, offers many possibilities to operate in HCCI mode while the battery can be recharged. As a result the rule-based and the optimal strategies result in almost equal fuel economy benefits and great synergies between the electric motor and the multimode engine. On the other hand, the HWFET displays an average load demand right above the HCCI regime and virtually no regeneration events. This leads to extended periods of time during which torque assist can be used to facilitate HCCI operation. However, for the rule-based strategies this translates into substantial battery discharge which is harmful for overall fuel economy. Therefore, in such a case battery SOC needs to be incorporated into the mode switching decision. Finally, the aggressive US06 cycle results in a load demand which is too high and can rarely be achieved by HCCI together with the ISG. As a result there are no significant synergies between mild HEV and SI/HCCI multimode engine despite several battery regeneration events over the course of the drive cycle. In future work the analysis can be extended by incorporating automatic transmissions and the combined optimization of gearshifts, engine torque and combustion modes.

Acknowledgment

The authors wish to thank (a) Dr. Patrick Gorzelic for helpful discussions on the SI/HCCI combustion mode switches, (b) the company CPT for providing ISG efficiency maps, and (c) Drs. Kim and Siegel for valuable discussions on battery and HEV modeling.

Appendix A. Details on vehicle model

Main parts of the vehicle model were described in Section 2 with additional details following here. See Fig. 1 for a block diagram of the system.

A.1. Engine

The response of the engine is modeled as first-order system with time constant $\tau_e = 0.09$ s, parameterized with throttle snap experiments:

$$\frac{d}{dt}T_e = \frac{1}{\tau_e}(u_e - T_e). \tag{A.1}$$

A.2. ISG and electric auxiliaries

The efficiency map f_m of the belt-driven ISG is modeled based on steady-state data. It computes the electric power of the motor $P_{m,el}$ as a function of mechanical power P_m and ω_m:

$$P_m = T_m \cdot \omega_m \tag{A.2}$$

$$P_{m,el} = f_m(P_m, \omega_m). \tag{A.3}$$

In case of the conventional vehicle the ISG is used as a conventional alternator to generate power for the electric auxiliary load, here assumed constant $P_{al} = 1250$ W. Therefore the associated commanded torque to the ISG $u_{m,al}$ is

$$u_{m,al} = -\frac{f_m^{-1}(P_{al}, \omega_m)}{\omega_m} \tag{A.4}$$

using the inverse of the ISG's efficiency f_m as well as the speed of the ISG $\omega_m = \gamma_b \omega_e$ with belt-ratio $\gamma_b = 2.5$. In the mild HEV the ISG is also used for regenerative braking with associated command $u_{m,r}$. If stronger deceleration is requested than available by the ISG, the friction brake is used, controlled by the modified brake signal $\hat{u}_b$. The sum of all ISG torque commands is then:

$$u_m = u_{m,al} + u_{m,c} + u_{m,r}. \tag{A.5}$$

The torque response of the ISG T_m is modeled as first-order system with time constant $\tau_m = 0.0043$ s:

$$\frac{d}{dt}T_m = \frac{1}{\tau_m}(u_m - T_m). \tag{A.6}$$

A.3. Battery

The battery power is drawn by the auxiliary load P_{al} and the ISG $P_{m,el}$:

$$P_b = P_{al} + P_{m,el}. \tag{A.7}$$

The battery behavior is described by an equivalent circuit model with I_c and U_c cell current and voltage, respectively (Guzzella & Sciarretta, 2007):

$$U_c = U_{OC}(\xi) - R_i(\xi, I_c) \cdot I_c \tag{A.8}$$

$$I_c = \frac{P_b}{n_s n_p U_c} \tag{A.9}$$

The battery consists of $n_p = 1$ cells in parallel and $n_s = 14$ in series, each cell with a capacity of $Q_c = 5$ A h. With an operating voltage of 48 V this translates to a nominal battery capacity of 240 W h. The open-circuit voltage U_{OC} and the internal resistance R_i are implemented as look-up tables based on steady-state data. They are functions of the battery's state-of-charge (SOC) ξ and, in case of R_i, the direction of I_c. The influence of battery temperature on U_{OC} and R_i is neglected. The battery's only state SOC is modeled applying Coulomb-counting (Guzzella & Sciarretta, 2007):

$$3600 \cdot Q_c \frac{d}{dt}\xi = -I_c. \tag{A.10}$$

A.4. Engine control unit (ECU)

Besides all the functionality for the supervisory control the ECU also translates pedal position u_a to desired engine torque T_{des}. In addition it contains an idle speed controller which maintains

800 RPM and makes the start/stop decision.

A.5. Drivetrain

The drivetrain is described by a hybrid dynamic system. It includes two discrete states, locked and slipping clutch, with transitions mainly determined by clutch pedal position u_{cl} and static clutch friction torque $T_{cl} = f(u_{cl})$. In addition, three continuous states are used to describe velocity v as well as driven and non-driven wheels. More information on the drivetrain model can be found in Nüesch et al. (1981).

A.6. Driver

The driver model is based on gain-scheduled PI controllers and uses accelerator, brake, and clutch pedal as well as gear, u_a, u_b, u_{cl}, and u_g, respectively, to track predetermined trajectories of reference velocity and gear, v_{ref} and g_{ref}, respectively.

References

Ahn, K., Whitefoot, J., Babajimopoulos, A., Ortiz-Soto, E., & Papalambros, P. (2012). Homogeneous charge compression ignition technology implemented in a hybrid electric vehicle: System optimal design and benefits analysis for a power-split architecture. *Proceedings of the Institution of Mechanical Engineering, Part D: Journal of Automobile Engineering 227*, 87–98.

Borhan, H., Vahidi, A., Philipps, A. M., Kuang, M. L., Kolmanovsky, I. V., & Di Cairano, S. (2012). MPC-based energy management of a power-split hybrid electric vehicle. *IEEE Transactions on Control Systems Technology*, *20*(3), 593–603.

Cairns, A., & Blaxill, H. (2005). The effects of combined internal and external exhaust gas recirculation. In *SAE*, no. 2005-01-0133.

Chasse, A., Corde, G., Del Mastro, A., & Perez, F. (2010). Online optimal control of a parallel hybrid with after-treatment constraint integration. In: *VPPC* (pp. 1–6).

Dec, J., & Sjöberg, M. (2003). A parametric study of HCCI combustion - the sources of emissions at low loads and the effects of GDI fuel injection. In *SAE*, no. 2003-01-0752.

Delorme, A., Rousseau, A., Wallner, T., Ortiz-Soto, E., Babajimopoulos, A., & Assanis, D. (2010). Evaluation of homogeneous charge compression ignition (HCCI) engine fuel savings for various electric drive powertrains. In *EVS-25*.

Farrell, J., & Stevens, J. (2006). Second law analysis of high efficiency low emission gasoline engine concepts. In *SAE*, no. 2006-01-0491.

Gao, Z., Conklin, J., Daw, C., & Chakravarthy, V. (2010). A proposed methodology for estimating transient engine-out temperature and emissions from steady-state maps. *International Journal of Engine Research*, *11*, 137–151.

Gorzelic, P. (2015). *Modeling and model-based control of multi-mode combustion engines for closed-loop SI/HCCI mode transitions with cam switching strategies* (Ph.D. thesis). University of Michigan, May.

Gorzelic, P., Shingne, P., Martz, J., Stefanopoulou, A., Sterniak, J., & Jiang, L. (2016). A low-order adaptive engine model for SI-HCCI mode transition control applications with cam switching strategies. *International Journal of Engine Research*, *17*(4), 451–468. http://dx.doi.org/10.1177/1468087415585016.

Guzzella, L., & Sciarretta, A. (2007). *Vehicle propulsion systems, introduction to modeling and optimization*. Berlin, Heidelberg: Springer.

Hellström, E., & Stefanopoulou, A. (2013). Cyclic variability and dynamical instabilities in autoignition engines with high residuals. *IEEE Transactions on Control Systems Technology*, *21*(5), 1527–1536.

Jade, S., Hellström, E., Larimore, J., Jiang, L., & Stefanopoulou, A. (2016). Controlled load and speed transitions in a multi-cylinder recompression HCCI engine. *IEEE Transactions on Control Systems Technology*, *23*, http://dx.doi.org/10.1109/TCST.2014.2346992 (in press).

Kelly, J., Scanes, P., & Bloore, P. (2014). Specification and design of a switched reluctance 48V belt integrated starter generator B-ISG for mild hybrid passenger car application. In *SAE*, no. 2014-01-1890.

Kulzer, A., Hathout, J.-P., Sauer, C., Karrelmeyer, R., Fischer, W., & Christ, A. (2007). Multi-mode combustion strategies with CAI for a GDI engine. In: SAE, no. 2007-01-0214.

Lawler, B., Ortiz-Soto, E., Gupta, R., Peng, H., & Filipi, Z. (2011). Hybrid electric vehicle powertrain and control strategy optimization to maximize the synergy with a gasoline HCCI engine. In *SAE*, no. 2011-01-0888.

Ma, T., Zhao, H., Li, J., & Ladommatos, N. (2001). Experimental investigation of controlled auto-ignition (CAI) combustion in a 4-stroke multi-cylinder gasoline engine and drive cycle simulations. In *Proceedings of IFP international congress* (pp. 115–124).

Nüesch, S. (2015). *Analysis and control of multimode combustion switching sequence* (Ph.D. thesis). University of Michigan, November.

Nüesch, S., & Stefanopoulou, A. (2015). Is it economical to ignore the driver? A case study on multimode combustion. In *ASME DSCC*.

Nüesch, S., & Stefanopoulou, A. (2016a). Multimode combustion in a mild hybrid electric vehicle. Part 2: Three-way catalyst considerations. *IFAC Control Engineering Practice*, this issue.

Nüesch, S., & Stefanopoulou, A. (2016b). Mild HEV with multimode combustion: Benefits of a small oxygen storage. In *IFAC AAC*.

Nüesch, S., Hellström, E., Jiang, L., & Stefanopoulou, A. (2013). Influence of transitions between SI and HCCI combustion on driving cycle fuel consumption. In *ECC* (pp. 1976–1981).

Nüesch, S., Sterniak, J., Jiang, L., & Stefanopoulou, A. (2015). On beneficial mode switch decisions based on short-term engine load prediction. In *IFAC E-COSM*.

Nüesch, S., Gorzelic, P., Jiang, L., Sterniak, J., & Stefanopoulou, A. (2016). Accounting for combustion mode switch dynamics and fuel penalties in drive cycle fuel economy. *International Journal of Engine Research*, *17*(4), 436–450. http://dx.doi.org/10.1177/1468087415584713.

Najt, P., & Foster, D. (1983). Compression-ignited homogeneous charge combustion. In *SAE*, no. 830264.

Onori, S., & Serrao, L. (2011). On adaptive-ECMS strategies for hybrid electric vehicles. In *RHEVE* (pp. 1–7).

Ortiz-Soto, E., Assanic, D., & Babajimopoulos, A. (2012). A comprehensive engine to drive-cycle modeling framework for the fuel economy assessment of advanced engine and combustion technologies. *International Journal of Engine Research*, *13*, 287–304.

Rick, A., & Sisk, B. (2015). A simulation based analysis of 12V and 48V microhybrid systems across vehicle segments and drive cycles. In *SAE*, no. 2015-01-1151.

Thring, R. (1989). Homogeneous-charge compression ignition (HCCI) engines. In *SAE*, no. 892068.

Willand, J., Nieberding, R., Vent, G., & Enderle, C. (1998). The knocking syndrome: Its cure and its potential. In *SAE*, no. 982483.